Computational sub-structure analysis of multidimensional detonation waves

Ralf Deiterding

Computer Science and Mathematics Division, Oak Ridge National Laboratory

Governing equations

We solve the inhomogeneous Euler equations for multiple species that read

$$\mathbf{q}_t + \nabla \cdot \mathbf{f}(\mathbf{q}) = \mathbf{s}(\mathbf{q}) \qquad (1)$$

with vector of state $\mathbf{q} = (\rho_1, \ldots, \rho_K, \rho u_1, \ldots, \rho u_d, \rho E)^T$ and flux functions

$$\mathbf{f}_n(\mathbf{q}) = (\rho_1 u_n, \ldots, \rho_K u_n, \rho u_1 u_n + \delta_{1n} p, \ldots, \rho u_d u_n + \delta_{dn} p, u_n(\rho E + p))^T .$$

The equation of state follows Dalton's law and the ideal gas law

$$p = \sum_{i=1}^{K} p_i = \mathcal{R}T \sum_{i=1}^{K} \frac{\rho_i}{W_i}$$

with the caloric equation

$$h = \sum_{i=1}^{K} Y_i\, h_i(T) , \qquad h_i(T) = h_i^0 + \int_{T^0}^{T} c_{pi}(\sigma) d\sigma$$

which requires computation of $T = T(\rho, e)$ from the implicit equation

$$\sum_{i=1}^{K} \rho_i h_i(T) - \rho e - \mathcal{R}T \sum_{i=1}^{K} \frac{\rho_i}{W_i} = 0 .$$

For chemistry, the source term is $\mathbf{s}(\mathbf{q}) = (W_1\, \dot\omega_1, \ldots, W_K\, \dot\omega_K, 0, \ldots, 0, 0)^T$ with the reaction rates for detailed kinetics

$$\dot\omega_i = \sum_{j=1}^{J} (\nu_{ji}^r - \nu_{ji}^f) \left[k_j^f \prod_{l=1}^{K} \left(\frac{\rho_l}{W_l}\right)^{\nu_{jl}^f} - k_j^r \prod_{l=1}^{K} \left(\frac{\rho_l}{W_l}\right)^{\nu_{jl}^r} \right] .$$

In here, all results were obtained with a mechanism for $H_2 - O_2 - Ar$ combustion with 34 elementary reactions and 9 species.

Numerical methods

Numerical source term incorporation and extension to multiple dimensions are done with the method of fractional steps. $\longrightarrow$ Numerical decoupling of hydrodynamic and chemical time steps.

Time-explicit 2nd order TVD shock-capturing method for thermally perfect gases:

In most cells an approximate Riemann solver with numerical flux function

$$\mathbf{F}(\mathbf{Q}_l, \mathbf{Q}_r) = \frac{1}{2}\left(\mathbf{f}(\mathbf{Q}_l) + \mathbf{f}(\mathbf{Q}_r) - \sum_{\iota=1}^{3} |s_\iota| \mathbf{W}_\iota \right)$$

with $s_1 = \hat u_1 - \hat c$, $s_2 = \hat u_1$, $s_3 = \hat u_1 + \hat c$ is used. The waves $\mathbf{W}_\iota$ are defined as

$$\mathbf{W}_1 = a_1 \hat{\mathbf{r}}_1 , \; \mathbf{W}_2 = \sum_{m=2}^{K+2} a_m \hat{\mathbf{r}}_m , \; \mathbf{W}_3 = a_{K+3} \hat{\mathbf{r}}_{K+3},$$

where

$$a_1 = \frac{\Delta p - \hat\rho \hat c \Delta u_1}{2\hat c^2} , \; a_{i+1} = \Delta \rho_i - \hat Y_i \frac{\Delta p}{\hat c^2} , \; a_{K+2} = \hat\rho \Delta u_n , \; a_{K+3} = \frac{\Delta p + \hat\rho \hat c \Delta u_1}{2\hat c^2} ,$$

and

$$\begin{aligned} \hat{\mathbf{r}}_1 &= (\hat Y_1, \ldots, \hat Y_K, \hat u_1 - \hat c, \hat u_2, \hat H - \hat u_1)^T, \\ \hat{\mathbf{r}}_{i+1} &= (\delta_{1i}, \ldots, \delta_{Ki}, \hat u_1, \hat u_2, \hat u_1^2 + \hat u_2^2 - \hat\phi_i/(\hat\gamma - 1))^T, \\ \hat{\mathbf{r}}_{K+2} &= (0, \ldots, 0, 1, \hat u_2)^T, \\ \hat{\mathbf{r}}_{K+3} &= (\hat Y_1, \ldots, \hat Y_K, \hat u_1 + \hat c, \hat u_2, \hat H + \hat u_1)^T. \end{aligned}$$

with the usual Roe average given by $\hat v := \frac{\sqrt{\rho_l} v_l + \sqrt{\rho_r} v_r}{\sqrt{\rho_l} + \sqrt{\rho_r}}$ for $u_n, Y_i, T, h_i, H := E + p/\rho$ and $\hat\rho := \sqrt{\rho_l \rho_r}$ and the specific averages

$$\hat\gamma := \frac{\hat c_p}{\hat c_v} \quad \text{with} \quad \hat c_{\{p/v\}} = \sum_{i=1}^{K} \hat Y_i \hat c_{\{p/v\}i} , \quad \hat c_{\{p/v\}i} = \frac{1}{T_r - T_l} \int_{T_l}^{T_r} c_{\{p,v\}i}(\tau)\, d\tau$$

and

$$\hat\phi_i := (\hat\gamma - 1)\left(\frac{\hat u_1^2 + \hat u_2^2}{2} - \hat h_i \right) + \hat\gamma \frac{\mathcal{R}}{W_i} \hat T , \quad \hat c := \left(\sum_{i=1}^{K} \hat Y_i \hat\phi_i - (\hat\gamma - 1)(\hat u_1^2 + \hat u_2^2 - \hat H) \right)^{1/2} .$$

The entropy correction reads

$$|\bar s_\iota| = \begin{cases} |s_\iota| , & |s_\iota| \ge 2\eta , \\ |s_\iota^2|/(4\eta) + \eta , & |s_\iota| < 2\eta \end{cases}$$

and is applied in 1d to $\iota = 1, 3$ with $\eta = \frac{1}{2}(|u_{1,r} - u_{1,l}| + |c_r - c_l|)$, where in 2d and 3d a multidimensional evaluation of η for all fields is used as carbuncle fix. Example:

$$\tilde\eta_{j,k+\frac12} = \max\left\{ \eta_{j+\frac12,k}, \eta_{j-\frac12,k}, \eta_{j,k+\frac12}, \eta_{j-\frac12,k+1}, \eta_{j+\frac12,k+1} \right\}$$

$j-\frac12,k+1$ | $j,k+\frac12$ | $j+\frac12,k+1$ | $j-\frac12,k$ | $j+\frac12,k$

The correction

$$\mathbf{F}_i^\star = \mathbf{F}_\rho \cdot \begin{cases} Y_i^l , & \mathbf{F}_\rho \ge 0 , \\ Y_i^r , & \mathbf{F}_\rho < 0 \end{cases}$$

ensures the positivity of the mass fractions Y_i. If internal energy or pressure in the intermediate states $\mathbf{Q}_l^\star = \mathbf{Q}_l + \mathbf{W}_1$ and $\mathbf{Q}_r^\star = \mathbf{Q}_r - \mathbf{W}_3$ are unphysical, i.e. $\rho_{l/r}^\star \le 0$ or $e_{l/r}^\star \le 0$, the HLL flux

$$\mathbf{F}(\mathbf{Q}_l, \mathbf{Q}_r) = \begin{cases} \mathbf{f}(\mathbf{Q}_l) , & 0 < s_1 , \\ \dfrac{s_3 \mathbf{f}(\mathbf{Q}_l) - s_1 \mathbf{f}(\mathbf{Q}_R) + s_1 s_3 (\mathbf{Q}_r - \mathbf{Q}_l)}{s_3 - s_1} , & s_1 \le 0 \le s_3 , \\ \mathbf{f}(\mathbf{Q}_r) , & 0 > s_3 , \end{cases}$$

with the wave speed estimation $s_1 = \min(u_{1,l} - c_l, u_{1,r} - c_r)$, $s_3 = \max(u_{1,l} + c_l, u_{1,r} + c_r)$ is used.

Source term integration:

- Standard solver for stiff ODE's, e.g., semi-implicit Rosenbrock-Wanner method
- Automatic stepsize adjustment to allow for an efficient treatment of chemical time scales smaller than the global time-step

Blockstructured AMR

Locally high resolution, which is essential for the accurate computation of detonation waves, is achieved by blockstructured Adaptive Mesh Refinement (AMR).

- Discretization necessary only for single rectangular grid
- Spatial and temporal refinement, no global time step restriction
- Blockstructured data guarantees high computational performance
- Non-conformal finite volumes unavoidable and require special treatment

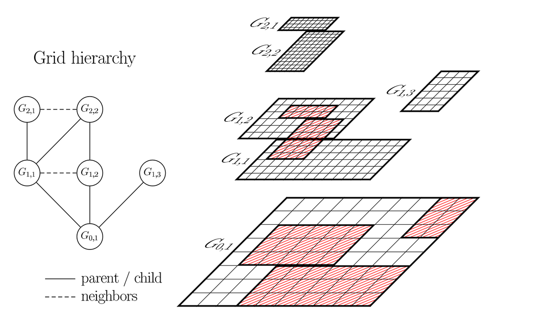

Our framework AMROC provides a generic object-oriented implementation of the blockstructured AMR method that is applicable to any explicit FV scheme for (1):

- Parallel hierarchical data structures employ MPI library
- Data follows "floor plan" of a single Grid Hierarchy.
- Data of all levels resides on same node $\longrightarrow$ most AMR operations are local
- Neighboring grids are synchronized transparently even over processor borders when boundary conditions are applied
- Distribution algorithm: Generalization of Hilbert's space-filling curve

Refinement indicators

Physically motivated refinement is achieved through scaled gradients

$$|w(\mathbf{Q}_{j+1,k}) - w(\mathbf{Q}_{jk})| > \epsilon_w , \; |w(\mathbf{Q}_{j,k+1}) - w(\mathbf{Q}_{jk})| > \epsilon_w , \; |w(\mathbf{Q}_{j+1,k+1}) - w(\mathbf{Q}_{jk})| > \epsilon_w$$

or estimating the leading-order term of the local error of quantity w by Richardson extrapolation

$$\tau_{jk}^w := \frac{|w(\bar{\mathcal{Q}}_{jk}(t + \Delta t)) - w(\mathcal{Q}_{jk}(t + \Delta t))|}{2^{o+1} - 2} .$$

In practice, we use the criterion

$$\frac{\tau_{jk}^w}{\max(|w(\mathcal{Q}_{jk}(t + \Delta t))|, S_w)} > \eta_w^r$$

that combines relative and absolute error.

Verification: Detonation ignition in a shock tube

Shock-induced detonation ignition of a hydrogen-oxygen-argon mixture at molar ratios 2:1:7 in a 1d shock tube closed at the left end.

- Insufficient resolution leads to inaccurate results
- Reflected shock is captured by the FV scheme correctly at all resolutions, but the detonation approximation is resolution dependent as can be seen in time t_m, when both waves merge
- Fine mesh necessary in the induction zone at the head of the detonation and AMR is highly suitable to reduce the compute time

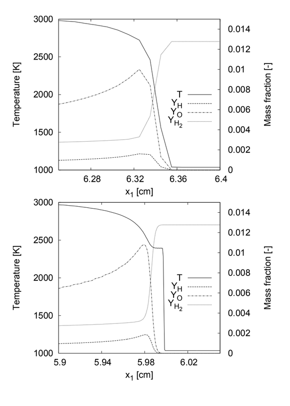

Approximation of the detonation wave at $t = 170\,\mu$s for the uniform resolutions $\Delta x_1 = 100\,\mu$m and $\Delta x_1 = 6.25\,\mu$m ($\sim$ 24 Pts/l_{ig}).

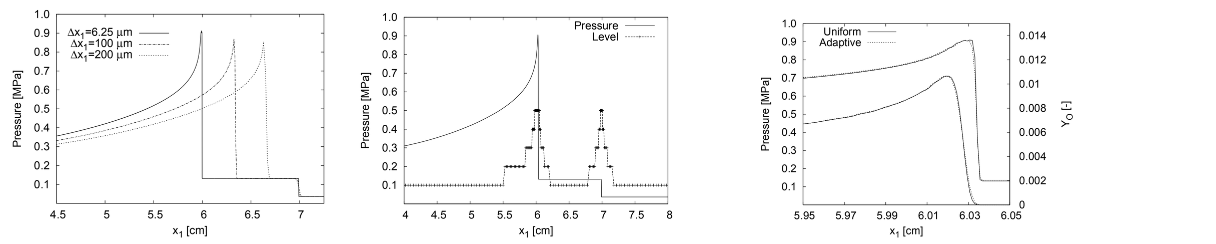

Left: Comparison of pressure distribution at $t = 170\,\mu$s for different mesh sizes. Middle: Domains of refinement levels. Right: Direct comparison of the distributions of p and Y_O in the detonation wave with a uniform simulation.

$\Delta x_1[\mu m]$	Uniform Cells	$t_m[\mu s]$	Time [s]	Adaptive l_{max}	r_l	$t_m[\mu s]$	Time [s]
400	300	166.1	31				
200	600	172.6	90	2	2	172.6	99
100	1200	175.5	277	3	2,2	175.8	167
50	2400	176.9	858	4	2,2,2	177.3	287
25	4800	177.8	2713	4	2,2,4	177.9	393
12.5	9600	178.3	9472	5	2,2,2,4	178.3	696
6.25	19200	178.6	35712	5	2,2,4,4	178.6	1370

Comparison of uniformly refined and dynamic adaptive simulations run on a single CPU of a Intel Xeon 3.4 GHz processor.

Y_i	$S_{Y_i} \cdot 10^{-4}$	$\eta_{Y_i}^r \cdot 10^{-3}$
O_2	10.0	2.0
H_2O	7.8	8.0
H	0.16	5.0
O	1.0	5.0
OH	1.8	5.0
H_2	1.3	2.0

$\epsilon_\rho = 0.07\,\mathrm{kg\,m^{-3}}$, $\epsilon_p = 50\,\mathrm{kPa}$

Refinement indicator values for the one-dimensional ignition problem.

Embedding of complex domains

Usage of a signed distance function φ for efficient implicit boundary representation on the hierarchical Cartesian mesh.

- $\varphi = 0$ marks the boundary, boundary normal $\mathbf{n} = \nabla\varphi / |\nabla\varphi|$
- Our current implementation evaluates φ in the midpoints only and uses mesh cells directly to prescribe boundary conditions $\longrightarrow$ proper AMR refinement of the boundary necessary
- Non-oscillating, 1st order accurate interpolation/extrapolation to construct ghost cell values
- Mirroring of the primitive values ρ_i, $\mathbf{u}$, p and inversion of normal velocity component by $\mathbf{u}' = (2\mathbf{w} \cdot \mathbf{n} - \mathbf{u} \cdot \mathbf{n})\mathbf{n} + (\mathbf{u} \cdot \mathbf{t})\mathbf{t} = 2((\mathbf{w} - \mathbf{u}) \cdot \mathbf{n})\mathbf{n} + \mathbf{u}$

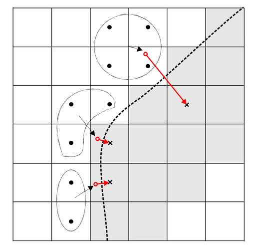

Interpolation from interior cells to construct mirrored values in ghost cells (gray).

Verification: Shock-induced combustion around a sphere

A spherical projectile of radius 1.5 mm travels with constant velocity v_I = 2170.6 m/s through a hydrogen-oxygen-argon mixture (molar ratios 2:1:7) at 6.67 kPa and T = 298 K and exhibits shock-induced combustion ignition.

- Cylindrical symmetric simulation on AMR base mesh of 70×40 cells
- Comparison of 3-level computation with refinement factors 2,2 ($\sim$ 5 Pts/l_{ig}) and a 4-level computation with refinement factors 2,2,4 ($\sim$ 19 Pts/l_{ig}) at t = 350 μs
- Higher resolved computation captures combustion zone visibly better and at slightly different position (see below)

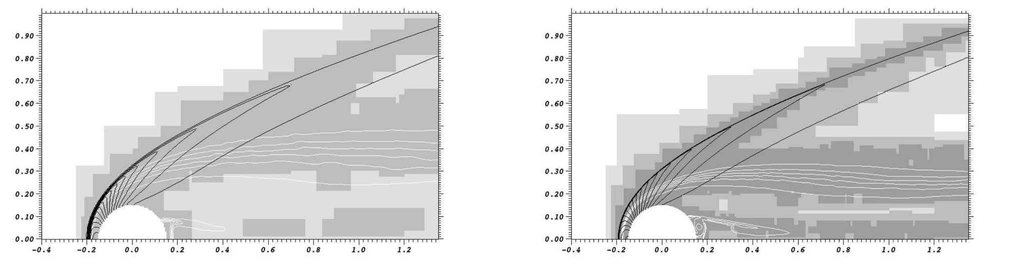

Iso-contours of p (black) and Y_{H_2} (white) on domains of different refinement levels (gray) at t = 350 μs for a 3-level computation with $r_{1,2} = 2$ (left) and a 4-level computation with $r_{1,2} = 2, r_3 = 4$ (right).

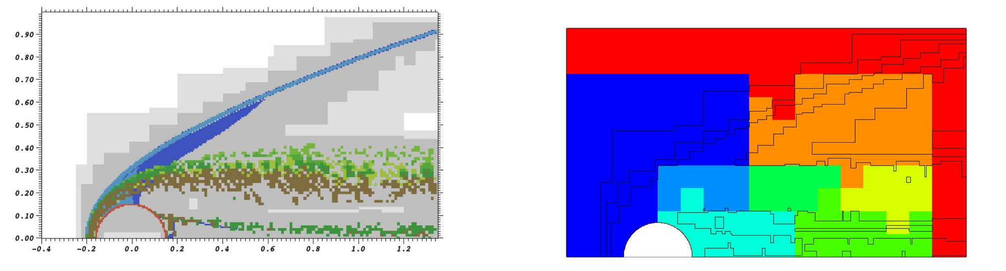

Left: Active refinement indicators on $l = 2$ at $t = 350\,\mu$s. Blue: ϵ_ρ, light blue: ϵ_p, green shades: $\eta_{Y_i}^r$, red: embedded boundary. Right: Domain decomposition to 8 processors for the 4-level hierarchy depicted in the graphic above.

Task	4 Procs Time [s]	%	8 Procs Time [s]	%	16 Procs Time [s]	%
Fluid dynamics	22374	34.6	11261	32.3	5742	26.7
Chemical kinetics	25280	39.1	12455	35.8	6291	29.2
Boundary setting	7758	12.0	5888	16.9	5761	26.8
Embedded boundary	5429	8.4	2839	8.2	1703	7.9
Recomposition	3210	5.0	1919	5.5	1623	7.5
Misc	638	0.9	456	1.3	416	1.9
Total / Speed-up	64689		34818	1.86	21536	1.62

Breakdown of computational costs for parallel 4-level simulations with $r_{1,2,3} = 2$ running from $t = 150\,\mu$s to $t_e = 400\,\mu$s.

Y_i	$S_{Y_i} \cdot 10^{-4}$	$\eta_{Y_i}^r \cdot 10^{-4}$
O_2	10.0	4.0
H_2O	5.8	3.0
H	0.2	10.0
O	1.4	10.0
OH	2.3	10.0
H_2	1.3	4.0

$\epsilon_\rho = 0.02\,\mathrm{kg\,m^{-3}}$, $\epsilon_p = 16\,\mathrm{kPa}$

Refinement indicator values for simulating shock-induced combustion around the projectile.

Cellular detonation and triple point structures

Self-sustaining detonations are inherently unstable and exhibit transverse pressure waves that propagate perpendicular to the detonation front. The transverse waves form evolving triple point patterns at the detonation front with severely enhanced pressure, temperature and thereby reaction. Despite considerable experimental efforts, a general model for the instability and the detailed flow field in triple points in detonations is not available yet.

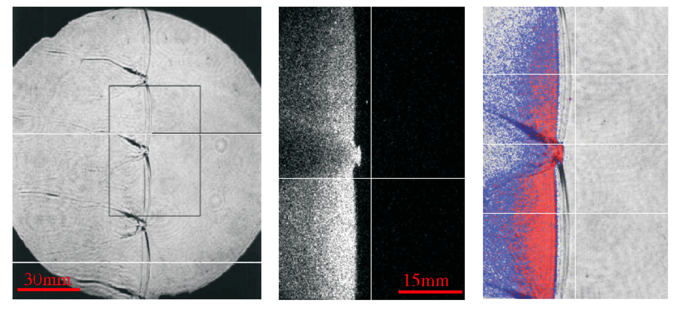

Schlieren and PLIF images of a regularly oscillating detonation front in hydrogen-oxygen-argon (image courtesy J. E. Shepherd, Graduate Aeronautical Laboratory, California Institute of Technology).

Objective of this work is to decipher the detailed hydrodynamic flow conditions in triple point sub-structures under periodic and transient conditions. In experiments, basically two different configurations have been qualitatively distinguished.

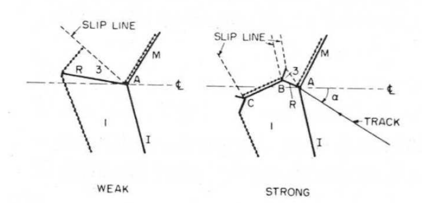

Experimentally known triple point structures.

Regular detonation structures in 2d

- Mixture: $H_2 : O_2 : Ar$ at molar ratios 2:1:7 at initially 298 K and 10 kPA
- Initialization with Chapman-Jouguet ZND solution and an irregular pocket to quickly trigger symmetry breaking. Tube width 3.2 cm
- Simulation until a *single* perturbation has developed into *two* regularly oscillating cells with width $\lambda = 1.6$ cm
- 67.6 Pts/l_{ig}. 4 additional refinement levels (2,2,2,4) on base mesh 2000×128
- Computation of triple point trajectories by tracking the magnitude of the vorticity vector on a uniform mesh at level 1

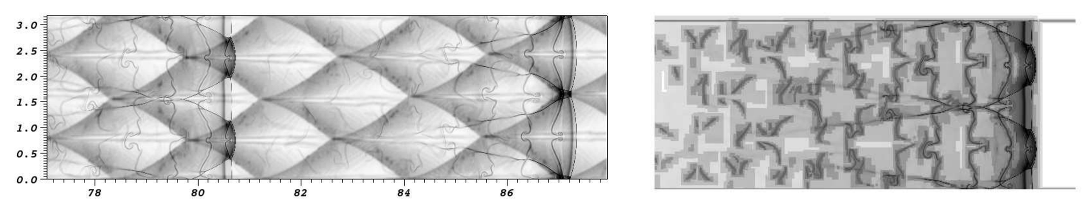

Left: Oscillating detonation front on computed triple points tracks. Right: Schlieren plot on refinement levels.

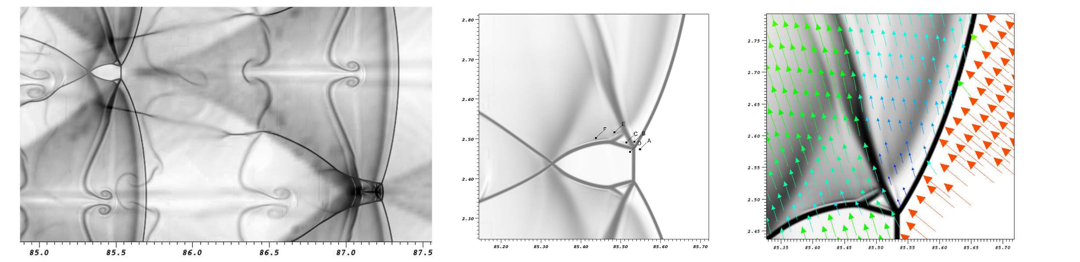

Left: Front on triple point tracks. 10 μs between snapshots (marked with open squares in (M_s, Φ_1)-plane, cf. right column). Middle and right: Clearly established Double-Mach reflection pattern shortly before triple point collision.

Only the strong structure appears in the simulations and can clearly be identified as a double-Mach reflection pattern.

	p/p_0	ρ/ρ_0	T [K]	q[m/s]	α	γ	M
A	1.00	1.00	298	1775	-39.5	1.557	5.078
B	31.45	4.17	2248	447	-64.4	1.487	0.477
C	31.69	5.32	1775	965	-64.4	1.500	1.153
D	19.17	3.84	1487	1178	-73.2	1.509	1.533
E	35.61	5.72	1856	901	-67.9	1.497	1.053
F	40.61	6.09	1987	777	-70.0	1.494	0.880

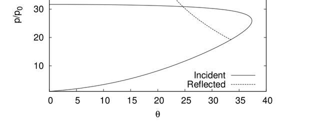

Values shortly before triple point collision in frame of reference of primary triple point. Inflow (A), Mach stem (B), reflected wave (C), incident shock (D), 2nd reflected (E), 2nd Mach stem (F). (q, α) are the polar coordinates of the velocity vector in the Galilean frame of reference. Right: shock polars for first triple point in left table.

Cellular structures in 3d

- $H_2 : O_2 : Ar/2 : 1 : 7$ at 6.67 kPA with cell width $\lambda = 3$ cm in 3d and 2d (not shown)
- High-resolution simulation of the quarter of a rectangular detonation cell
- Simulation under Galilean transformation $\longrightarrow$ inflow of unreacted gas with CJ velocity
- 44.8 Pts/l_{ig}. 2 additional refinement levels (2,4) on base mesh $400 \times 24 \times 24$, adaptive Simulation uses $\sim 18 \cdot 10^6$ cells instead of $118 \cdot 10^6$ (uniform)
- $\sim$ 55,000 h CPU on 128 Compaq Alpha processors

Regularly oscillating detonations that exhibited a strong structure in 2d, show only the weak structure in 3d as the transverse wave is weaker as in 2d. The resulting structure in 3d can be identified as a transitional Mach reflection.

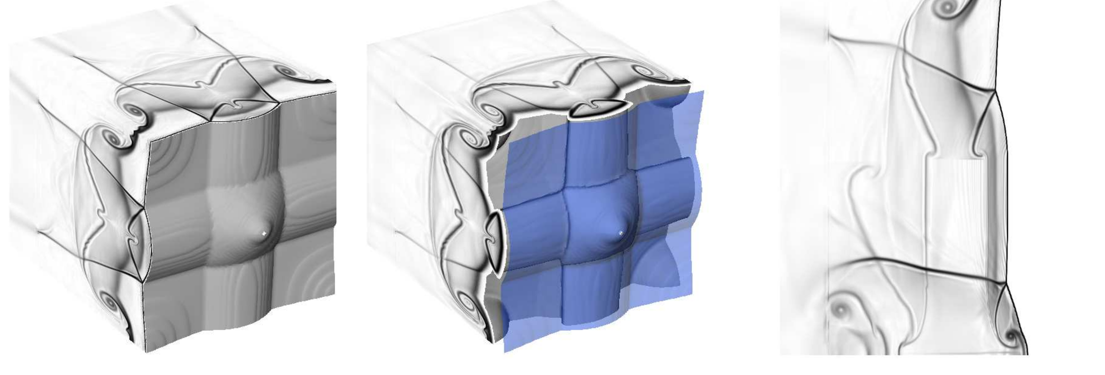

Left, middle: Schlieren plots of ρ (left) and Y_{OH} in the first half of a detonation cell. Data displayed is for 5.0 cm $< x_1 <$ 7.0 cm and mirrored at $x_2 = 0$ and $x_3 = 0$. The blue of ρ visualizes the induction length. Right: Planes with schlieren plots of ρ through the origin normal to x_2 and x_3-axis unfolded exhibit the transitional Mach structure behind the triple points, which is characterized by a kink instead of secondary triple point on the transverse wave.

Detonation structure in smooth pipe bends

- Initialization with 5 regularly oscillating detonation cells in $H_2 : O_2 : Ar/2 : 1 : 7$ at initially 298 K and 10 kPa, tube with 8 cm
- Pipe bend with radius 8 cm. Angle $\theta = \{15^o, 30^o, 45^o, 60^o\}$
- 67.6 Pts/l_{ig}. 4 additional refinement levels with factors (2,2,2,4)
- Adaptive computations use $\sim 7 \cdot 10^6$ cells ($\sim 5 \cdot 10^6$ on highest level) instead of $\sim 1.2 \cdot 10^9$ cells (uniform grid)
- $\sim$ 70,000 h CPU each on 128 CPUs Pentium-4 2.2 GHz

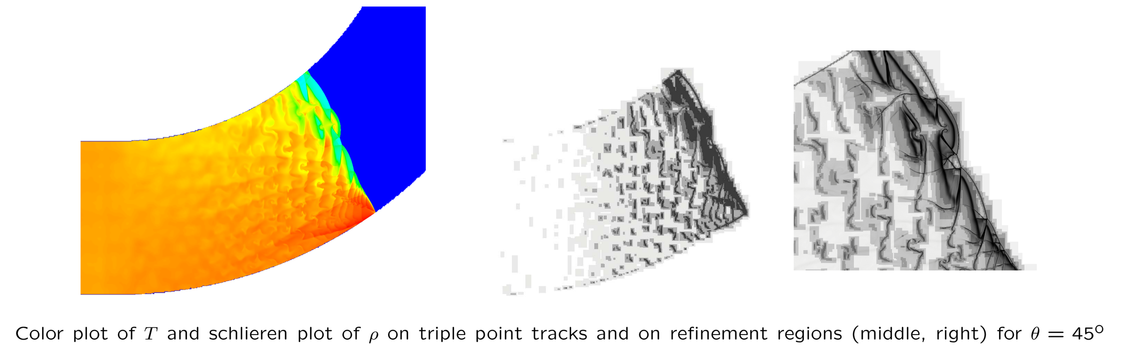

Color plot of T and schlieren plot of ρ on triple point tracks and on refinement regions (middle, right) for $\theta = 45^o$ after $t = 150\,\mu$s simulated time.

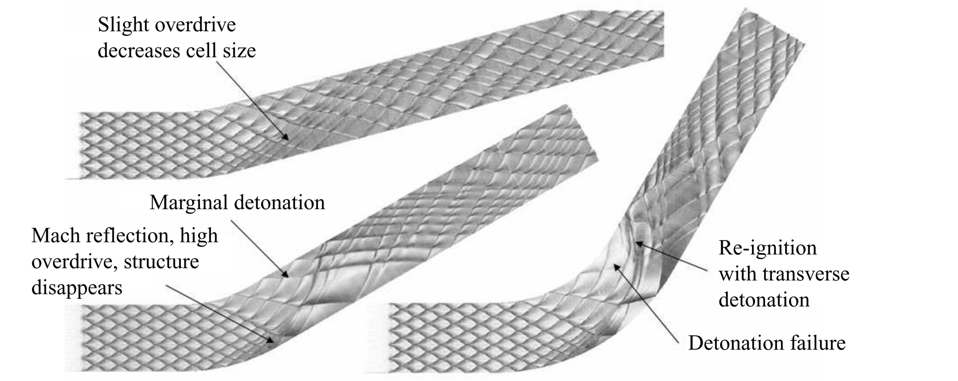

Triple point tracks for $\theta = 15^o$ (left, top), $\theta = 30^o$ (left, bottom), and $\theta = 60^o$ (right) display the fundamental flow features.

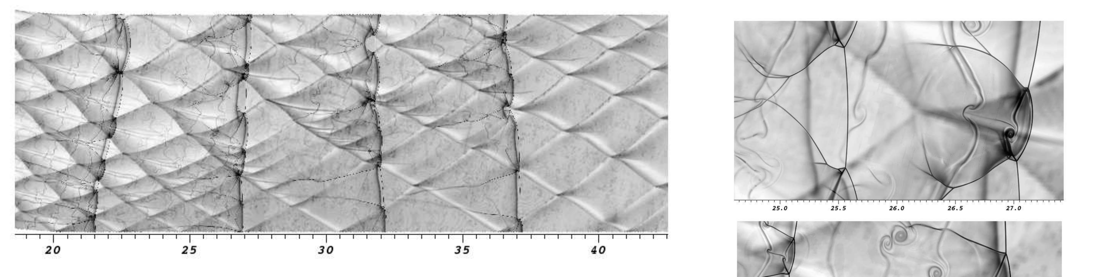

Top: Front on triple point tracks for $\theta = 15$ and 110 μs, 140 μs, 170 μs, 200 μs simulated time. Right, top: Strengthening of double-Mach reflection pattern (solid squares in (M_s, Φ_1)-plane) under expansion at 130 μs and 140 μs. Right, bottom: Weakening transitional Mach reflection in over-driven region (open circles in (M_s, Φ_1)-plane) at 130 μs and 140 μs.

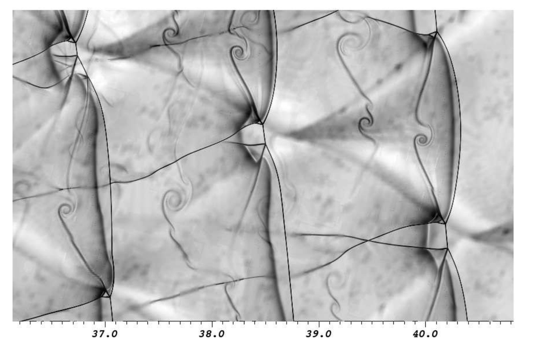

Triple point re-initiation with change from transitional to double-Mach reflection (solid circles in (M_s, Φ_1)-plane) when the oscillation becomes regular again after the bend, $\theta = 15$ at 200 μs, 210 μs, and 220 μs.

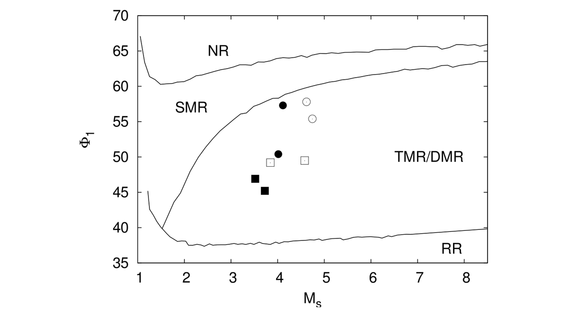

Domains and transition boundaries of different shock wave reflection phenomena. Frame of reference of first triple point. Φ_1 is angle between incident shock and vector (q, α), $M_s = sin(\Phi_1)M$. NR: no reflection, SMR: single Mach reflection, TMR/DMR: transitional/double-Mach reflection, RR: regular reflection.

Under transient boundary conditions, the regularly oscillating detonation exhibits both weak and strong triple point structures. Detailed quantitative triple point analysis for the thermally perfect, but non-reactive, $H_2 - O_2 - Ar$ mixture (using the oblique shock relations to transform the Eulerian data into the frame work reference of the primary triple point) indicates strongly:

- Triple point structures in self-sustained detonations exist only in the transitional and double-Mach, but not in the single-Mach reflection regime (cf. above (M_s, Φ_1)-plane)
- The relative strength $S = \frac{p_C - p_D}{p_D}$ of the transverse pressure wave primarily determines the reflection type
- A change of the reflection type happens especially in triple point collisions

Publications

R. D.. A parallel adaptive method for simulating shock-induced combustion with detailed chemical kinetics in complex domains, *Computers & Structures*, submitted, 2008.

R. D. Dynamically adaptive simulation of regular detonation structures using the Cartesian mesh refinement framework AMROC. *Int. Journal Computational Science and Engineering*, accepted and in press, 2008.